Symbiosis

www.symbiosisonlinepublishing.com
ISSN Online: 2372-0964

Research Article | SOJ Materials Science & Engineering | Open Access

# Primary Nano-Indentation Assessment of Low Entropy Nial-Cr Alloys

**C Mathiou, K Kyrtsidou, E Georgatis, AE Karantzalis***

*Department of Materials Science and Engineering, University of Ioannina, Greece*

**Received: July 05, 2021; Accepted: January 13, 2022; Published: January 17, 2022**

***Corresponding author:** AE Karantzalis, Department of Materials Science and Engineering, University of Ioannina, Greece, , E-mail: akarantz@uoi.gr*

## Abstract

Various (hypo-eutectic, eutectic and hypereutectic) NiAl – Cr alloys were assessed as far their dynamic nano-indentation based mechanical properties are concerned. Nano-indentation hardness, nano-indentation modulus of elasticity and nano-indentation elastic to overall absorbed energy ratio were calculated. Creep response was also examined under two different penetration depths. As far as the basic mechanical properties is concerned, it was found that the penetration depth and the applied load are the crucial parameters for the obtained values. The nature of the involved micro-constituents (primary or eutectic) also affects the mechanical response due to the different deformation mechanisms that can be expressed. The creep behaviour is considered to be affected by the microstructure, the penetration depth. Fundamental theories of power law creep and "sudden bursts" were adopted to explain the received results.

**Keywords**: Low Entropy Alloys; Dynamic Nanoindentation;, Indentation Creep

## Introduction

During the last decade, significant research effort has been conducted in the field of NiAl-based alloys and composite systems. The attractive properties of the particular intermetallic compound like its low density (5.9 g/cm$^3$ for the stoichiometric composition), good thermal expansion coefficient, comparable to that of Ni-based superalloys[1], and its high degree of thermodynamic stability due to its significantly negative enthalpy of mixing (-22 kJ/mol) make NiAl-based alloys potential candidates for high-temperature applications and for substituting various well-known superalloys[2-4]. The NiAl-Cr system, as part of the general endeavor for microstructural reinforcement of the NiAl-based alloys with the introduction of refractory elements, has attracted special interest [5]. Apart from, nevertheless, this specific field of superalloy's potential substitution, the entrance of High-Entropy Alloys in the metallurgical world, revealed another dimension of the importance of the Ni-Al-Cr elemental combination. Indeed, a significant amount of these new class alloys has been developed and assessed based on the Ni-Al-Cr core [6-11]. Tang et al. [2] presented an exceptional research work on clarifying the possible final microstructural configurations of the NiAl-Cr pseudo-binary system at various compositions, based on thermodynamic and kinetic calculations. Among the mechanical properties, creep resistance is considered as one of the most critical properties for various industrial applications, for both conventional and advanced alloys, including HEAs. The first systematic presentation of the creep behavior of various materials, evaluated by indentation techniques, was introduced by Li et al. [12]. At the beginning of their approach, two distinct areas below the indenter were identified: a hydrostatic pressure zone, where there is no plasticity, followed by an elastic-plastic region, where plastic deformation can occur and creep phenomena can accumulate. In this work, Li et al. [12] proposed various creep mechanisms: (a) the dislocation slip mechanism due to the development of high stresses within the elastic-plastic region (a mechanism prevailing especially at low temperatures), (b) the power law-type mechanism characterized by a mixed climbing-sliding function of dislocations, which is evident at high temperatures (the mechanism is mainly controlled by the highest temperatures), (c) the mechanism where the initial power law of dislocation climbing is sub-divided into a mixed climbing-sliding function of dislocations when high stresses are present along with high temperatures, and (d) creep due to diffusion, where the stress fields differences between the hydrostatic and the elastic-plastic zones create chemical potential gradients, which lead to atomic diffusion and material flow from the hydrostatic zone under the indenter, to the elastic-plastic zone near the sample's surface. This means volume diffusion in the case of monocrystalline material, as, in the case of polycrystalline samples, the material flow is facilitated by the slip caused by grain boundaries' diffusion. What is quite remarkable in the approach of Li et al. [12] is the fact that only the latter mechanism seems to depend on the externally applied load. It is important to note, however, that in this study, the effect of the pre-creep stage, through the loading rate, was not examined. Moreover, several other studies have also shown that grain size, applied load/penetration depth, loading rates and creep duration are the most critical parameters affecting

the material's creep response. In order to evaluate the creep response, these parameters were formulated in factors such as Indentation Size Effect (ISE) and Loading Rate Sensitivity (LRS) and were used in several different cases as in the work [13-18].

## Materials and Methods

Detailed description of the experimental procedure for the manufacturing and the microstructural characterization of the different alloys can be found in the work of Mathiou et al. [19] Dynamic indentation tests were performed using a Shimadzu DUH-211S nano-indenter with a standard Berkovich diamond tip at room temperature. Initial machine calibration was conducted on a fused silica standard to ensure the validity of the testing data. The load holding time was settled as 10 s, to determine whether a creep behavior occurred. Two indentation depth limits for each indent, (medium at 1000 nm and shallow at 500 nm) were selected, while the strain rate was kept constant at 0.05 s-1. Average values and standard deviation were calculated based on at least 10 trials for each specimen. For more details on the procedure to evaluate the creep assessment, the reader should address to the work of Karantzalis et al. [20].

## Results and Discussion

### Microstructural Features

The microstructures of the produced low-entropy alloys in lower and higher magnifications are presented in Figure 1. Table 1 summarizes the data provided by EDS mapping and point analysis associated with the different, actual phases being present on each individual alloy.A detailed description of the various phases present in each alloy would be out of the scope of the present effort and for further details the reader should refer to the work of Mathiou et al[19] where the phases' formation and solidification phenomena of these systems are in depth presented.

### Nano-indentation tests

Nano-indentation tests were conducted in almost all the produced low-entropy alloy. The objective of this approach was based on the investigation of the creep behaviour of each individual micro-constituent present in the final microstructure of the examined systems. As such, the examination was focused on the primary and the eutectic phases present in all alloy cases. More specifically, the primary and eutectic micro-constituents of the NiAl-25Cr, NiAl-33Cr, NiAl-40Cr and NiAl-60Cr low-entropy alloys were tested so as the basic creep parameters ($E_{IT,}$ HV and $n_{IT}$) and the load-displacement curves along with the derived data to be measured and analyzed. It has to be mentioned, though, that the composition of 80 at.% Cr was not included in the examined alloys, due to the small size of the NiAl phase in which the indentation measurements were not possible. However, this high Cr content hyper-eutectic alloy is represented by the NiAl-60Cr alloy.

Table 1: Elemental compositions of the different alloy systems after EDS mapping and point analysis for the overall and the individual phases being present in each case

| | | Atomic Percentage at.% | | |
|---|---|---|---|---|
| Al | | Ni | Cr | |
| NiAl-25Cr (hypo-eutectic) | NOMINAL | 37.50 | 37.50 | 25 |
| | ACTUAL | 32.53 | 41.54 | 25.93 |
| | LIGHT (PRIMARY) | 41.74 | 49.52 | 8.73 |
| | DARK | 11.13 | 62.94 | 25.92 |
| NiAl-33Cr (near eutectic) | NOMINAL | 33.50 | 33.50 | 33 |
| | ACTUAL | 28.56 | 37.82 | 33.62 |
| | LIGHT (PRIMARY) | 37.90 | 50.51 | 11.58 |
| | DARK | 9.68 | 28.92 | 61.40 |
| NiAl-40Cr (hyper-eutectic) | NOMINAL | 30 | 30 | 40 |
| | ACTUAL | 26.21 | 33 | 40.76 |
| | PRIMARY DARK | 11.88 | 10.70 | 77.42 |
| | PRIMARY LIGHT | 35.02 | 46.37 | 18.65 |
| NiAl-60Cr (hyper-eutectic) | NOMINAL | 20 | 20 | 60 |
| | ACTUAL | 16.72 | 23.07 | 60.21 |
| | LIGHT | 30.50 | 48.95 | 20.55 |
| | DARK | 8.81 | 9.22 | 81.97 |
| NiAl-80Cr (hyper-eutectic) | NOMINAL | 10 | 10 | 80 |
| | ACTUAL | 6.87 | 10.58 | 82.54 |
| | LIGHT | 30.70 | 55.87 | 13.43 |
| | DARK | 4.08 | 4.27 | 91.65 |

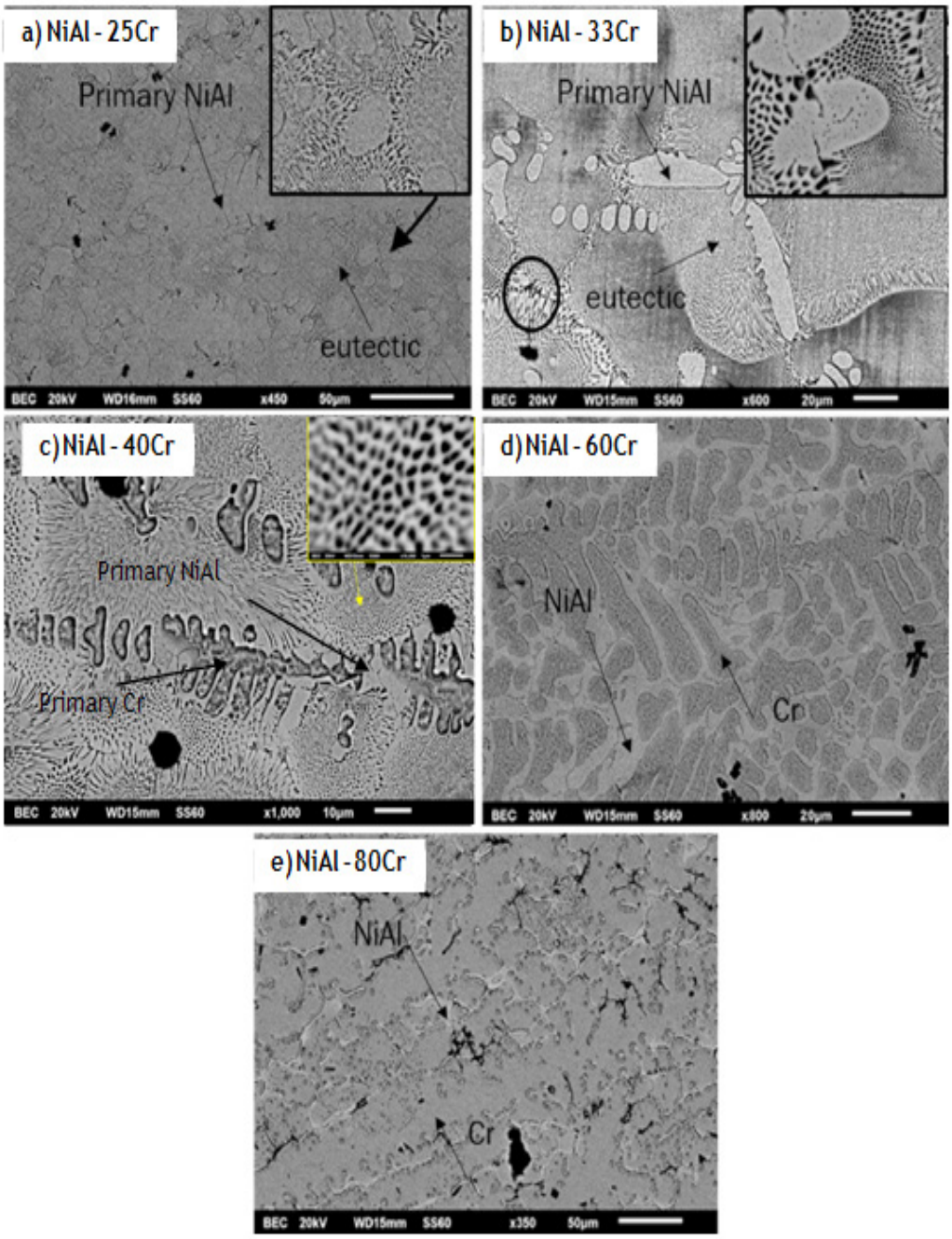


**Figure 1:** The panoramic view of the microstructure of the produced alloys: (a) NiAl-25Cr, (b) NiAl-33Cr, (c) NiAl-45Cr, (d) NiAl-60Cr and (e) NiAl-80Cr. Reconstruction after the work of Mathiou et al. [19]

## Calculation of basic parameters

The calculated values of the basic creep parameters for the individual micro-constituents (primary and eutectic phases) of the different examined systems for both the 500 nm and 1000 nm penetration depths, respectively, are presented in Tables 2 and 3. More specifically, the calculated parameters include the indentation modulus ($E_{IT}$), hardness (HV*) and the percentage of the absorbed elastic energy compared to the total energy absorbed during the test ($n_{IT}$).

Figure 2 shows the difference of the indentation hardness, ($E_{IT}$), measured for the primary constituent between the two different penetration depths (500 nm and 1000 nm) for all the examined alloys. The same analysis is also conducted for the eutectic micro-constituent in Figure3. It should be mentioned, though, that the following analysis does not include the primary phase in the NiAl-40Cr alloy and the eutectic phase in the NiAl-60Cr alloys, as it is already observed from the missing values in Tables 2 and 3 . The reason why is attributed to the very restricted area of the primary phase in the former case, making it difficult for the indenter to limit its penetration only within this short area, and the absence of the eutectic micro-constituent in the latter case. At this point, it has to be reminded that the primary phase of the NiAl-25Cr and NiAl-33Cr alloys is a NiAl-rich B2 phase, while the corresponding one for the NiAl-40Cr and NiAl-60Cr alloys is Cr-rich A2 phase.

From the data of Figure 2, it appears that there is a slight decrease concerning the indentation modulus value from the NiAl-25Cr to the NiAl-33Cr alloy, respectively. The reduction of $E_{IT}$ seems to be related to the lattice distortion decrease between the two alloys. In the case of the NiAl-33Cr, the lower value of δ (6.25 compared to 6.44 of the NiAl-25Cr alloy) is equivalent to the corresponding decrease of the elastic stress field within the crystal lattice, caused by the mixing of multiple different elements, and therefore, to the occurrence of a larger extent of elastic deformations for the same loading conditions, i.e. to a lower indentation modulus. The increased indentation modulus value in the case of the NiAl-60Cr alloy is justified by the presence of a Cr-rich solid solution primary phase, which is considered as one of the hardest metallic elements, thus, exhibiting a high $E_{IT}$ value. The tendency for different indentation modulus values between the three investigated alloys, seems to govern both depths of penetration (500 nm and 1000 nm). It has to be mentioned, though, that in all different alloy systems, the indentation modulus seems to decrease with increasing the penetration depth, i.e. in the case of 1000 nm. This behavior can be attributed to two different possible reasons: (a) the way the $E_{IT}$ parameter is calculated, according to which, the load and penetration depth parameters do not participate in the same proportional way (the penetration depth participates in a larger degree), and (b) the different distribution and extent of areas showing a hydrostatic-elastic and/or plastic behaviour under the indenter's surface, in conjunction with the penetration depth. More specifically, according to the literature [12,18,21], for swallow penetration depths, the extent of the plastic zone is limited compared to the hydrostatic-elastic area. As a result, plastic deformation at such swallow depths is limited, thus, providing steeper load-displacement curves, while their slope is a determining factor when measuring the indentation modulus.

Regarding the parameters' calculated values in the eutectic micro-constituent (Figure 3 and Tables 2 and 3) no specific trend can be expressed for the various systems. It seems, however, that the general trend for lower parameter's values at higher penetration depths still exists with the exception of the NiAl-33Cr alloy, which also exhibits the lowest values in terms of elasticity modulus. The main and vital difference between the eutectic and the primary phases is the fact that the eutectic micro-constituent consists of two distinct phases: a NiAl-rich B2 and a Cr-rich A2 phase, respectively, with an extremely fine cellular morphology. The discussion, thus, refers to nano-crystalline components and not to a single crystal as in the case of the primary phases. As Ma et al. [18] have extensively mentioned, the nano-structured nature of the examined phases, significantly changes the material's behaviour during nano-indentation tests, as mechanisms that are unconventional to plastic deformation, such as grain boundary migration and sliding of individual grains, may be activated, providing various combinations of elastoplastic deformation.

Figure 4 shows the hardness (HV*) measurements for the primary constituent at the two different penetration depths (500 nm and 1000 nm) for all the examined alloys. The same analysis is also conducted for the eutectic micro-constituent in Figure 5.

When the evaluation of the indentation hardness of the primary phases is concerned (Figure 5, Tables 2 and 3), it seems that there are no major differences between the values of the NiAl-25Cr and the NiAl-33Cr alloy systems. Besides, in both cases, the primary constituent is identified as a NiAl-rich B2 phase, and as such, big differences are not expected. A slight increase in its micro-hardness value is observed in the NiAl-60Cr alloy, which is, nevertheless, expected due to the nature of the primary phase (Cr-rich A2 phase), with the highest micro-hardness. As in the case of the indentation modulus, the micro-hardness values decrease with increasing penetration depth. This particular decrease, however, is in this case, as well, expected because during the indentation hardness calculation, the contribution of load and penetration depth is not proportional, with the penetration depth having a greater effect.

Similar observation with those of the indentation modulus are applied also when the indentation hardness of the eutectic micro-constituents is concerned. More specifically, the nano-crystalline nature of the participating phases may possibly lead to local deformation behaviours to the overall observed deformation. As in the case of the indentation modulus, the penetration depth seems to have a similar effect on the indentation hardness, as well, for the reasons explained previously. Interestingly, the NiAl-33Cr exhibits a similar behaviour to the previously investigated parameter $E_{IT,}$ exhibiting lower and reverse values of micro-hardness between the two penetration depths. The most likely explanation for this behaviour is probable correlated to the granulometry and size of the nano-structured eutectic

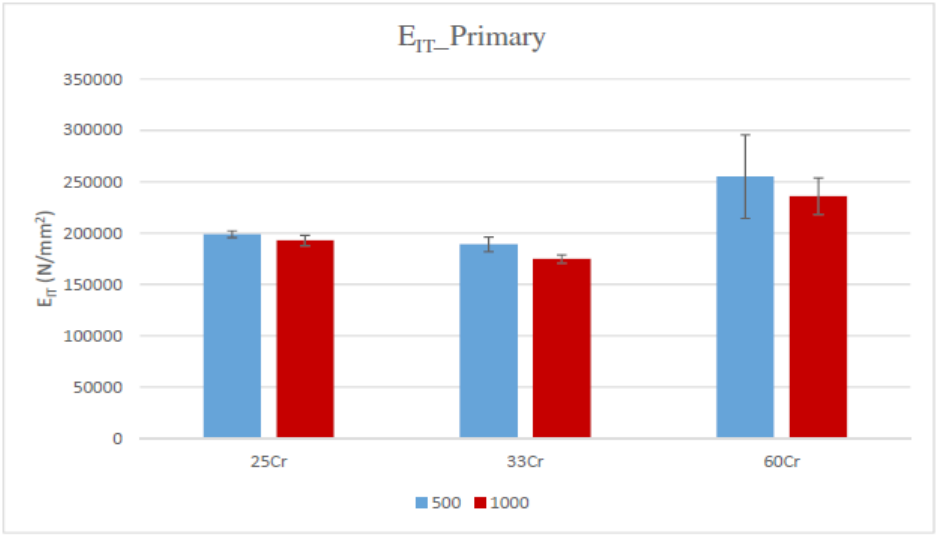


**Figure 2:** Indentation modulus ($E_{IT}$) of the primary phase for all the examined alloys in both penetration depths (500 nm and 1000 nm)

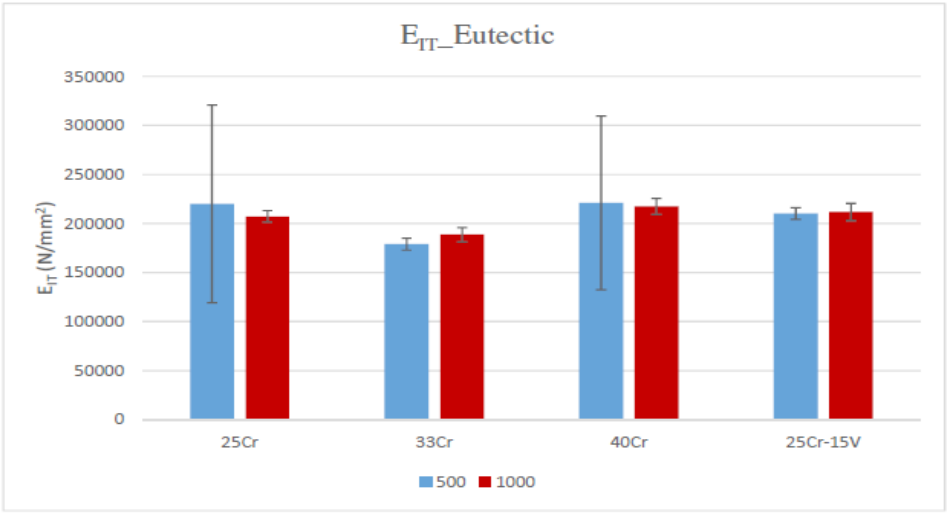


**Figure 3:** Indentation modulus ($E_{IT}$) of the eutectic phase for all the examined alloys in both penetration depths (500 nm and 1000 nm)

Table 2: Summarized values of $E_{IT}$, *HV** and $n_{IT}$ for the eutectic and primary phases of all the examined alloys at 500 nm penetration depth

| | | $E_{IT}$ (N/mm2) | HV* | $n_{IT}$ (%) |
|---|---|---|---|---|
| ***NiAl-25Cr*** | Eutectic | 220000 ± 100937 | 638.70 ± 20 | 26.53 ± 0 |
| | Primary | 199000 ± 3314 | 601.42 ± 12 | 26.97 ± 2 |
| ***NiAl-33Cr*** | Eutectic | 179000 ± 5962 | 404.97 ± 64 | 26.79 ± 10 |
| | Primary | 189000 ± 7179 | 640.05 ± 30 | 28.23 ± 1 |
| ***NiAl-40Cr*** | Eutectic | 221000 ± 88656 | 627.52 ± 11 | 24.23 ± 1 |
| | Primary | - | - | - |
| ***NiAl-60Cr*** | Eutectic | - | - | - |
| | Primary | 255000 ± 40647 | 695.04 ± 24 | 21.95 ± 2 |

phases. Although a clear indication of the size of the eutectic micro-constituent present in the NiAl-33Cr alloy, as well as its comparison with that of the NiAl-25Cr and NiAl-40Cr alloy systems, cannot be given by the SEM images, it is assumed that its size should be smaller than that of the other two systems, so that the sliding mechanisms of the nano-structured grains could give a more extensive plastic deformation. Consequently, the penetration depths would be greater leading to lower micro-hardness values as observed. However, further investigation is needed in order to clarify the above behaviour.

Figures 6 and 7 show the percentage of the absorbed elastic energy compared to the total energy absorbed during the test ($n_{IT}$), for the primary and the eutectic micro-constituents, respectively, at the two different penetration depths (500 nm and 1000 nm) for all the examined alloys.

In the case of the $n_{IT}$ calculations at the primary phases (Figure 6, Tables 2 and 3), it appears that all alloy systems follow the same trend of both the indentation modulus and hardness: The higher the modulus and hardness, the lower the energy due to elastic deformation. Although this finding seems to be oxymoronic, it, nevertheless, has a logical explanation. It is known that when the indentation modulus becomes greater, the load-displacement curve becomes steeper (due to a bigger slope with is attributed to the modulus of elasticity). This practically means that for bigger loads, the penetration depths are swallower. Consequently, the corresponding areas under the load-displacement curves, which express the energy due to the elastic deformation, become smaller and so do the respective energies. Another interesting point is the decrease of the ratio with the penetration depth, a fact that is completed expected, since with increasing the penetration depth, the area of plastic deformation increases, as well, i.e. the area of plastic deformation increases and as such, the ration decreases.

When the $n_{IT}$ calculations at the eutectic phases is concerned (Figure 7,Tables 2 and 3), not a specific trend is observed, which is probably associated with the nano-structured morphology they display. However, the effect of penetration depth on the $n_{IT}$ values, follows the same patterns as in the previous cases and is due to the same reasons discussed above.

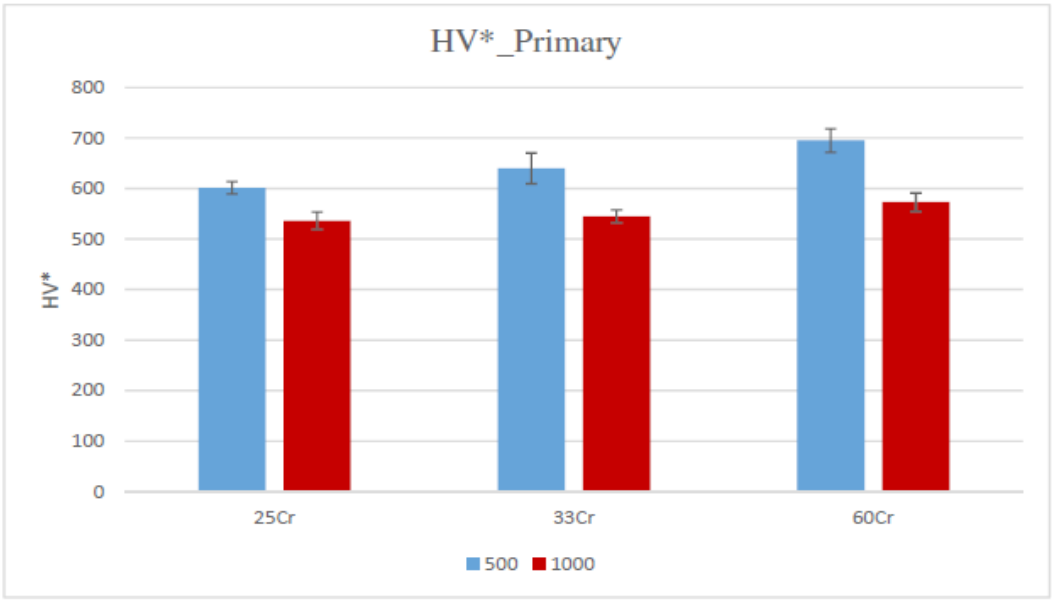


**Figure 4:** Indentation hardness (HV*) of the primary phase for all the examined alloys in both penetration depths (500 nm and 1000 nm)

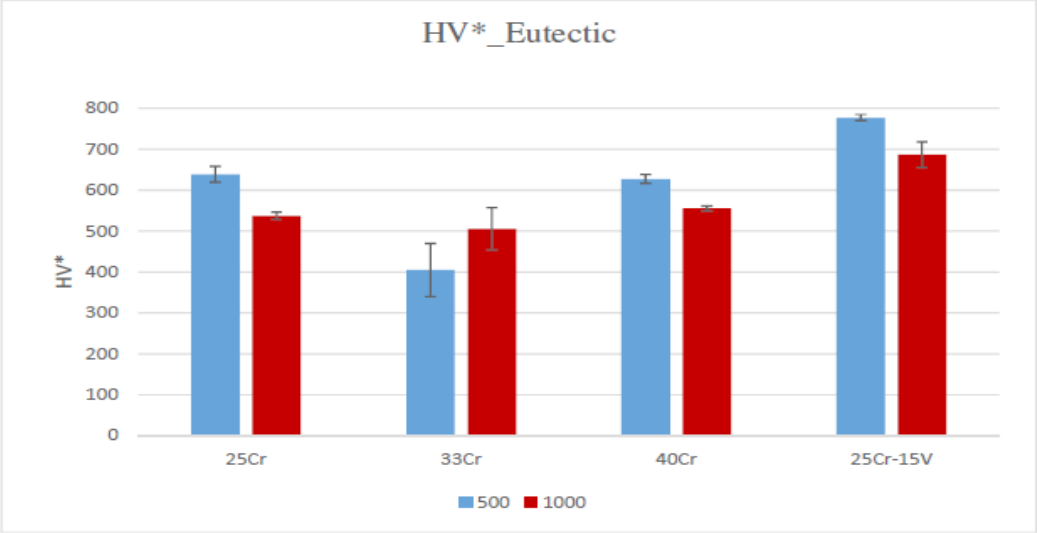


**Figure 5:** Indentation hardness (HV*) of the eutectic phase for all the examined alloys in both penetration depths (500 nm and 1000 nm)

Table 3: Summarized values ofEIT, HV* and $n_{IT}$ for the eutectic and primary phases of all the examined alloys at 1000 nm penetration depth

| | | $E_{IT}$ (N/mm²) | HV* | $n_{IT}$ (%) |
|---|---|---|---|---|
| ***NiAl-25Cr*** | Eutectic | 207280 ± 5827 | 537.55 ± 9 | 21.45 ± 1 |
| | Primary | 192850 ± 5120 | 536.22 ± 18 | 22.79 ± 1 |
| ***NiAl-33Cr*** | Eutectic | 188571 ± 7346 | 505.67 ± 52 | 23.61 ± 2 |
| | Primary | 174700 ± 4100 | 544.77 ± 13 | 24.60 ± 1 |
| ***NiAl-40Cr*** | Eutectic | 217320 ± 8270 | 555.40 ± 6 | 20.54 ± 1 |
| | Primary | - | - | - |
| ***NiAl-60Cr*** | Eutectic | - | - | - |
| | Primary | 236100 ± 17579 | 573.07 ± 18 | 19.46 ± 1 |

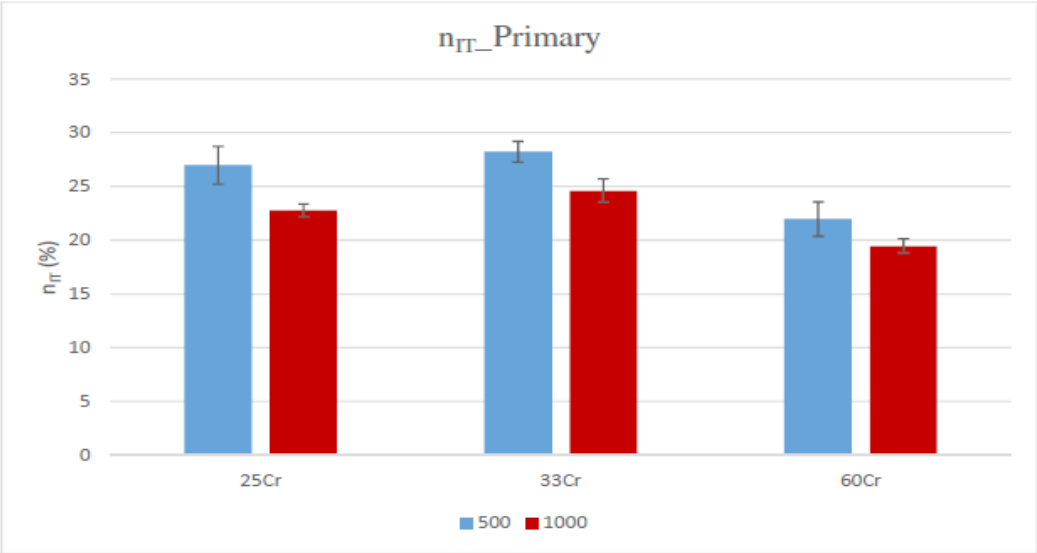


**Figure 6:** The percentage of the absorbed elastic energy compared to the total energy absorbed during the test ($n_{IT}$), of the primary phase for all the examined alloys in both penetration depths (500 nm and 1000 nm)

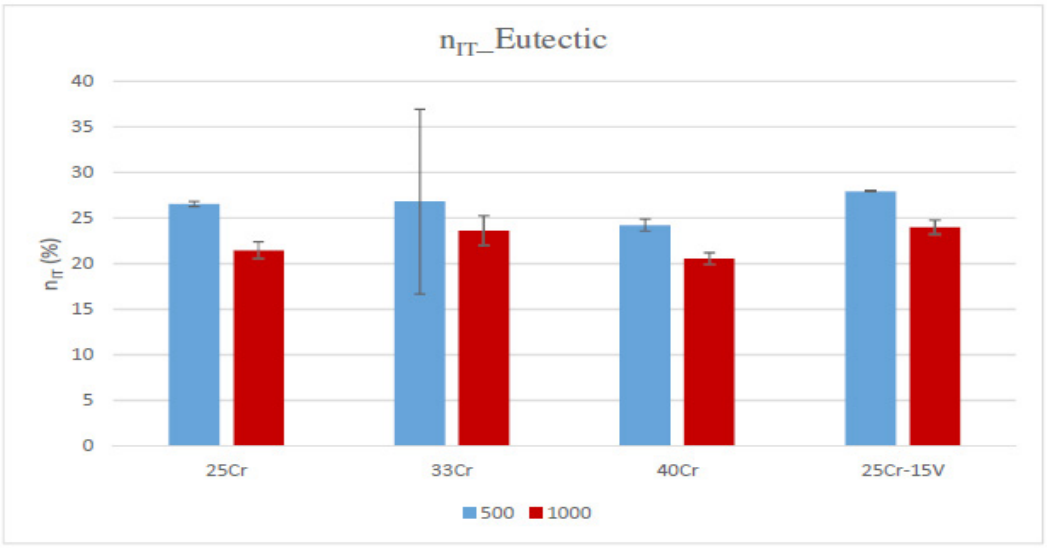


**Figure 7:** The percentage of the absorbed elastic energy compared to the total energy absorbed during the test ($n_{IT}$), of the eutectic phase for all the examined alloys in both penetration depths (500 nm and 1000 nm)

## Analysis of the creep curves

### a. Loading stage

The analysis of the creep behaviour was based on the work of Karantzalis et al. [20] where the reader should refer for further details. In order to receive a thorough analysis of the results concerning the alloys' creep behaviour, a detailed examination of the material's response during the loading stage prior to the creep stage is required. Figure 8 shows the loading curves of the primary constituent at a penetration depth of 500 nm, while Figure 9 shows the corresponding curves regarding the eutectic micro-constituent. In both cases, it is observed that all curves coincide, exhibiting a smooth evolution during testing, without the presence of localized gradations or small plateaus, known as "serrations" [16-18,21]. The presence of serrations during the loading stage signals the occurrence of creep phenomena during this stage, i.e. creep deformation prior to the holding stage (creep stage). A direct consequence of such behaviour is, according to the literature [17,22], the decrease of creep deformation at the creep stage.The morphology of the load-displacement curves of Figures 8 and 9 shows that no creep phenomena occur during loading. This is probably attributed to the relatively high loading rate which leads to typical work hardening conditions where dislocations multiply but do not move until the load is increased. Similar conclusions have been reported in the literature, as well [17,22]. Interestingly, the desired penetration depth of 500 nm in the case of the eutectic micro-constituent is achieved in values of load lower than those required for the primary phase. This behaviour can be possibly attributed to the relatively nano-structured morphology and the extremely fine size of the participating phases consisting the whole eutectic structure. The smaller the size, the bigger the probability of deformation, due to the relative movement/sliding of the phases between them or the migration of the grain boundaries. These two possible mechanisms are not present in the case of the primary constituent, where tests were performed within the interior of the grains far away from the interfacial regions, and as such extensive plastic deformation can occur [18]. Regarding the loading curves for both the primary and the eutectic phases at 1000 nm penetration depth (Figure 10 and 11) no difference in their morphology and shape is observed, compared to the corresponding ones for the case of 500 nm. Consequently, it could be assumed that similar phenomena and mechanisms govern the behavior of the alloys in this case as well. However, contrary to the case of 500 nm, at a higher penetration depth of 1000 nm, the eutectic micro-constituent does not exhibit the same ability in obtaining the desired depth. This is probably attributed to the reduced developed stresses, due to the nature of the experiment and the higher penetration depth, which may not be sufficient to activate the phase sliding or/and the grain boundaries migration mechanisms [14].

### b. Holding (Creep) stage

Figure 12 shows the time-displacement behaviour of the primary phase of all the investigated alloys at 500 nm penetration depth. A close examination of these curves reveals the presence of two types of curves that describe the alloys' creep behavior: (a) curves that are mostly governed by the power law creep behaviour, and (b) three curves that show a sharp increase in creep deformation, a phenomenon known in the literature as "sudden bursts" [23,24].

The occurrence of such phenomena where a sharp increase in creep deformation is observed, is, according to Bahr et al. [24] and Feng et al. [24], a result of the lack of formation of a critical dislocation density at the initial loading stage, prior to creep. Bahr et al. [23] and Feng et al. [24] claim that during the loading stage, the dislocations that are formed are not sufficient in order to effectively move and produce plastic deformation during the holding (creep) stage. However, on the onset of creep, under a

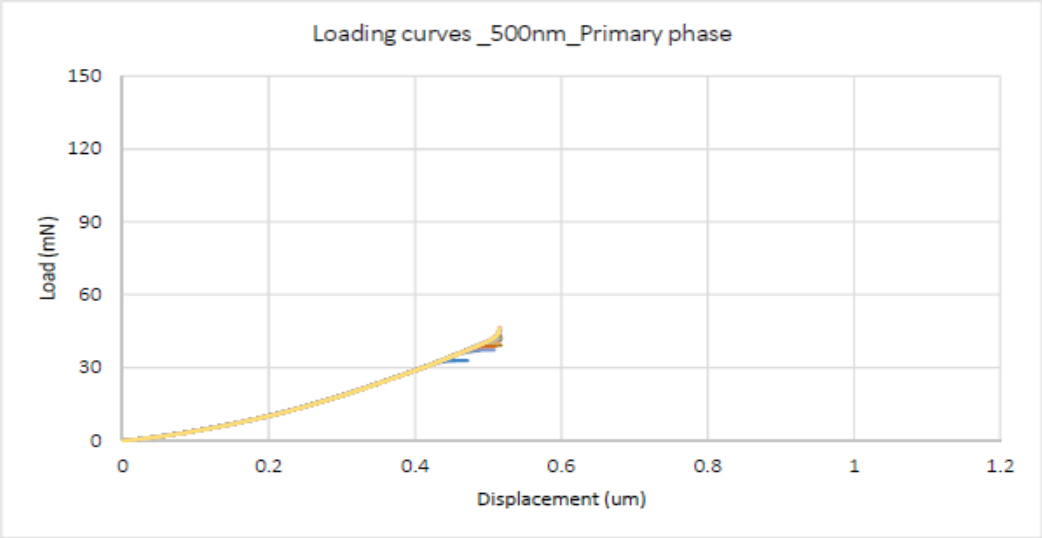


**Figure 8:** Loading curves of the primary phase at 500 nm penetration depth

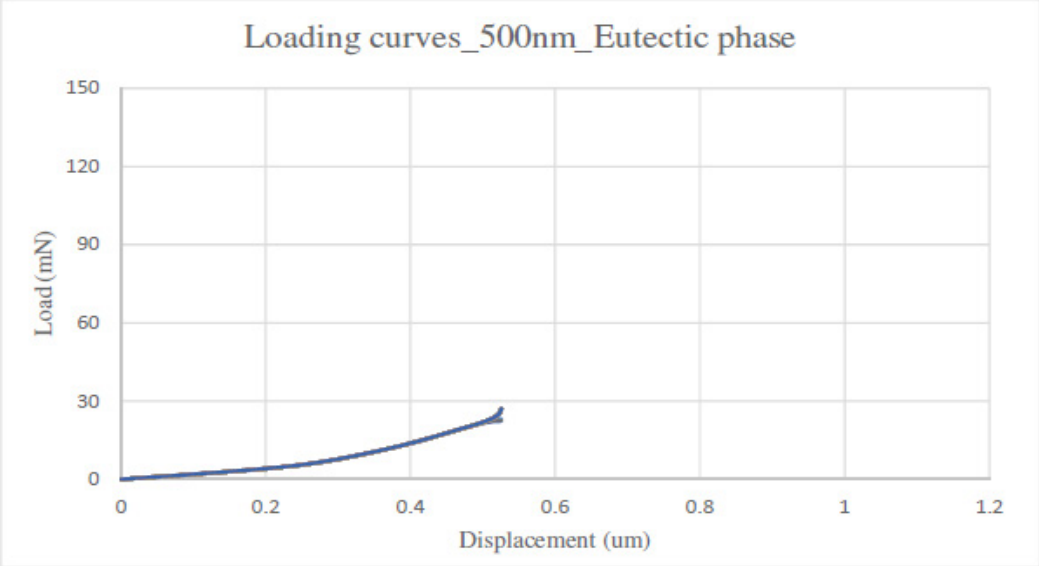


**Figure 9:** Loading curves of the eutectic phase at 500 nm penetration depth

constant load, the existing dislocations accumulate in the area under the indenter, locally increasing their density to higher levels than the critical density. As such, under the effect of the applied load and having exceeded their critical density, an instantaneous movement/displacement of all the dislocations occurs, providing this sharp deformation observed in Figure 12.

However, in the case of the primary phase at 500 nm penetration depth, the majority of the curves exhibits the typical morphology that the power law creep behaviour provides. For this given morphology, which has extensively been studied in the literature [16,18,22], the critical parameter calculated is the stress exponent, n, which expresses the creep deformation rate sensitivity due to the applied load [17,18,20]. Table 4 shows the calculated stress exponent values of the primary constituent at 500 nm penetration depth. In a following paragraph, a comparative analysis of the stress exponents, n, for the different penetration depths and the different micro-constituents will be made.

As for the corresponding results concerning the eutectic micro-constituent, Figure 13 shows the time-displacement curves of all the investigated alloys at 500 nm penetration depth. It is observed that there are no sharp deformation shifts and that all curves follow the typical power law, providing, thus, the ability to calculate the stress exponent, n, the values of which are

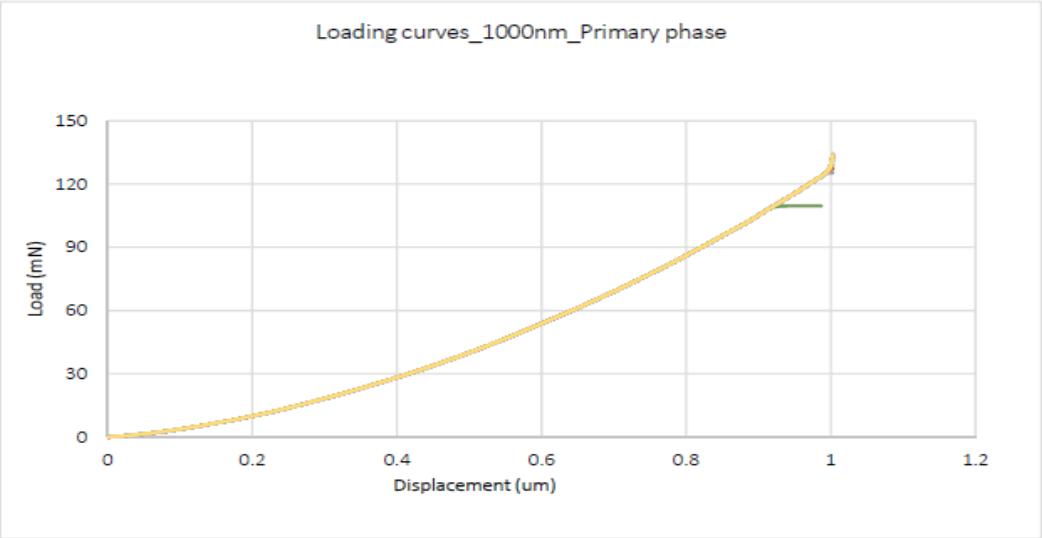


**Figure 10:** Loading curves of the primary phase at 1000 nm penetration depth

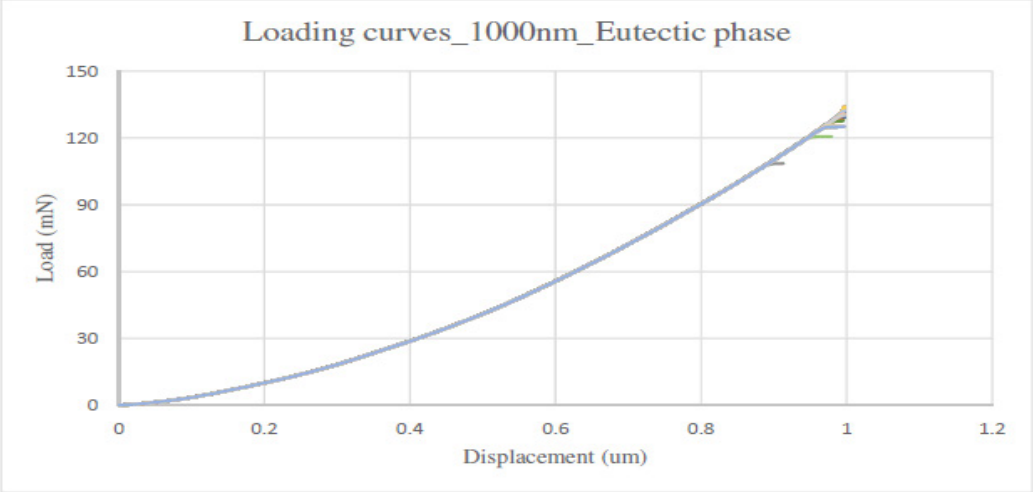


**Figure 11:** Loading curves of the eutectic phase at 1000 nm penetration depth

presented in Table 4.

Figure 14 shows the time-displacement curves of the primary phase for all the investigated alloys at 1000 nm penetration depth. In contrast to the previous case, with the swallower penetration depth of 500 nm, all curves follow the typical power law, and as such the calculation of the stress exponent, n, was made possible and is presented in Table 5.

Figure 15 shows the time-displacement curves of the eutectic phase for all the investigated alloys at 1000 nm penetration depth. It is observed that the majority of the curves are governed by the power law creep behaviour, and as such the calculated stress exponent values are presented in Table 5. However, there are some individual cases, where a sharp increase of the creep deformation is observed. The phenomena governing these sharp increases were, nonetheless, explained in a previous paragraph. In this case, however, additional deformation mechanisms may be involved, such as grain boundary migration and grain sliding. Either way, the eutectic micro-constituent needs further analysis. The creep displacement values of both the primary and the eutectic constituent for the two different penetration depths (500 nm and 1000 nm) are also displayed in Tables 4 and 5. It is observed that:

In the case of the primary phase, there is an increase in the creep displacement values from the NiAl-25Cr to the NiAl-33Cr. In both alloy systems, the primary constituent consists mainly of aNiAl-rich B2 phase, while different amounts of Cr is being dissolved within it. The creep displacement increase may be related to the lattice distortion parameter, δ, due to the fact that as

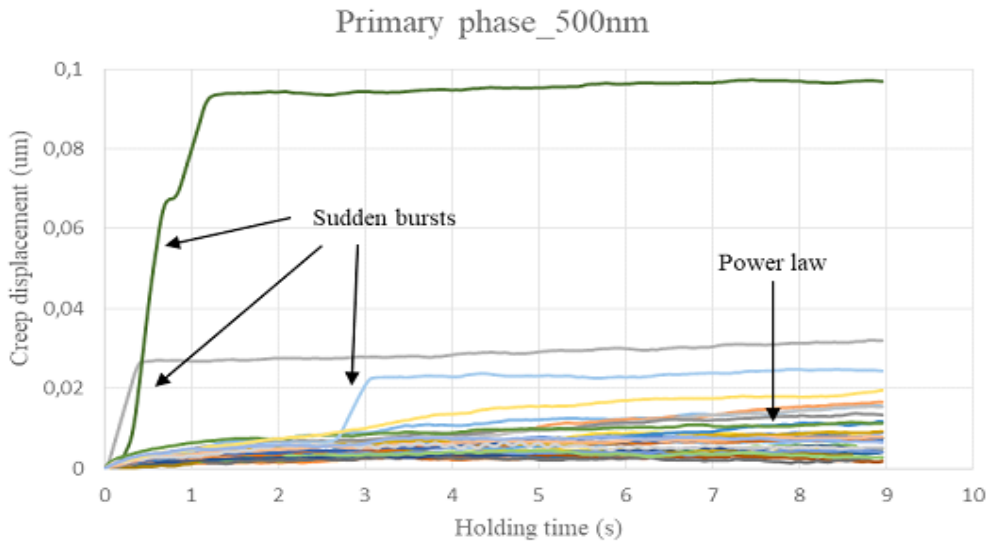


**Figure 12:** The indentation displacement as a function of time during the holding (creep) stage of the indentation tests for the primary phase at 500 nm penetration depth

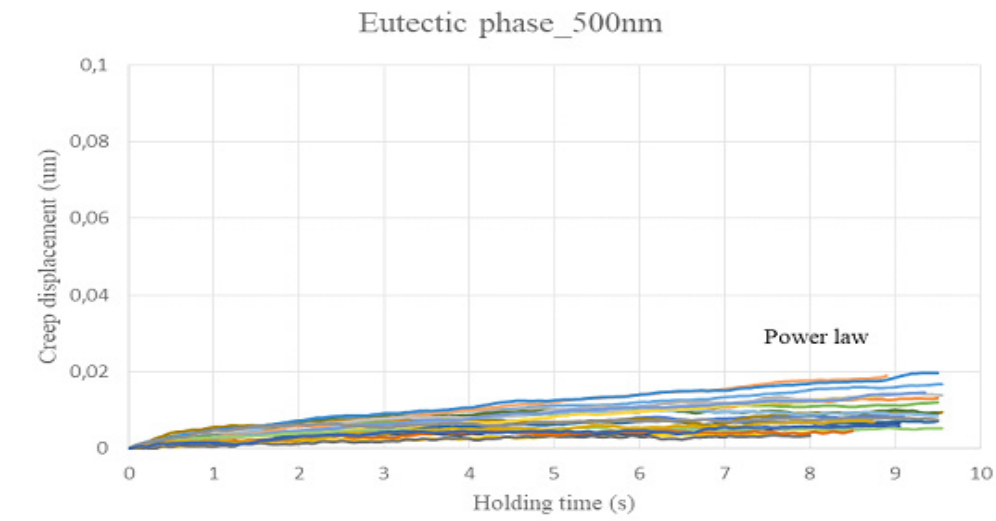


**Figure 13:** The indentation displacement as a function of time during the holding (creep) stage of the indentation tests for the eutectic phase at 500 nm penetration depth

Table 4: Summarized values of creep displacement, lattice distortion and stress exponent for the eutectic and primary phases of all the examined alloys at 500 nm penetration depth

| | | Creep displacement | Lattice distortion | Stress exponent |
|---|---|---|---|---|
| ***NiAl-25Cr*** | Eutectic | 11.26 ± 3 | - | 80.82 ± 2 |
| | Primary | 5.73 ± 3 | 6.70 | 105.87 ± 6 |
| ***NiAl-33Cr*** | Eutectic | 8.88 ± 2 | - | 66.26 ± 2 |
| | Primary | 10.73 ± 5 | 6.62 | 93.50 ± 4 |
| ***NiAl-40Cr*** | Eutectic | 10.91 ± 5 | - | 65.85 ± 2 |
| | Primary | - | - | - |

| | | | | |
|---|---|---|---|---|
| ***NiAl-60Cr*** | Eutectic | - | - | - |
| | Primary | 10.95 ± 5 | 6.35 | 60.59 ± 4 |

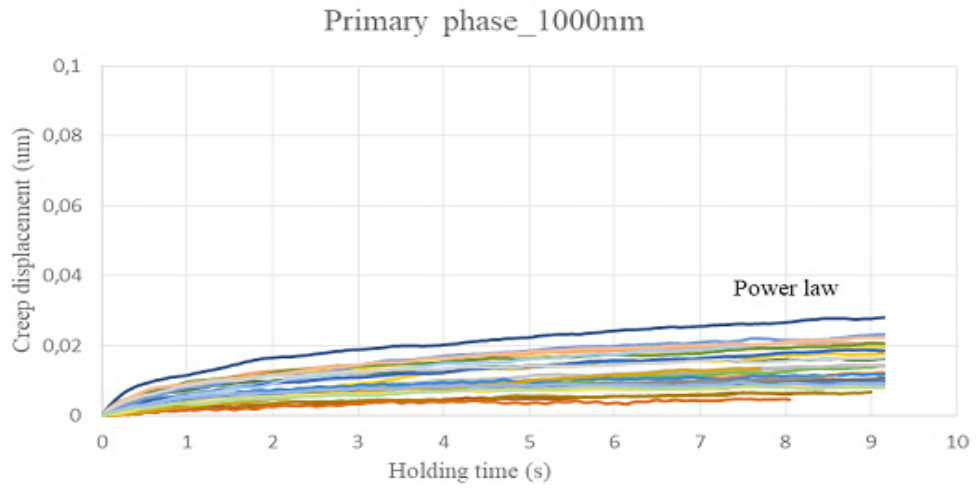


**Figure 14:** The indentation displacement as a function of time during the holding (creep) stage of the indentation tests for the primary phase at 1000 nm penetration depth

the displacement becomes bigger, the obstacles to the dislocation movement, which could provide plastic deformation, are increased, as well. As for the primary constituent of the NiAl-60Cr alloy, it cannot be compared to the previous cases, as it consists of a different Cr-rich A2 phase (with dissolved Al and Ni elements within its lattice).Regarding the eutectic micro-constituent, the creep displacement values do not show great differences. The microstructural complexity due to the participation of two nano-structured phases, makes the formulation of a generalized mechanism extremely difficult, and further research needs to be conducted.

Prior to the analysis of the stress exponent values, it should be emphasized that this exponent is a measure of the dependence of creep deformation rate on the applied load during the holding (creep) stage. In other words, it is practically a measure of how easy or not the creep deformation can occur. According to the data of Tables 4 and 5, the following observations can be made:

With respect to the penetration depth of 500 nm, the primary constituent shows a gradual decrease of its stress exponent values with increasing Cr content. It is also observed that the creep displacement generally increases with increasing Cr content, while at the same time, the lattice distortion, δ, values decrease. This observation indicates that the dislocation movement in a less distorted lattice, becomes much more easily, due to lower intensity elastic fields-obstacles, they encounter during their movement. This finding further implies that the creep displacement occurs much easier and exhibits reduced sensitivity to the applied external stress. This means that the deformation rate, in turn, does not show much dependence on the applied load, and as such, the stress exponent decreases. Based on the literature [14,18,20,22], these calculated values are attributed to dislocation sliding as the dominant mechanism concerning the dislocation movement, while for higher values, dislocation climbing plays also a supportive role.

In the case of the eutectic micro-constituent, the formulation of a mechanism that would explain the changes in the stress exponent values is very tricky. The calculated values are generally lower than those of the primary phase. This means that the creep deformation rate sensitivity to the applied load is lower, i.e. the creep deformation becomes easier. This behaviour is probably attributed to the microstructure of the eutectic micro-constituent, based on which, other mechanisms may be activated, such as the grain boundary migration and the grain sliding, that make the deformation much easier [12,18,22].

In the case of 1000 nm penetration depth the behaviour of the primary phase is reversed. More specifically, the increase of the Cr content leads to the increase of the stress exponent values, contrarily to the corresponding values at the penetration depth of 500 nm. The observed opposite behaviour may possibly be related to the different values of the applied external stress. Additionally, as described previously, in the case of 1000 nm depth, the indentation hardness values are lower than those of 500 nm. This practically justifies the higher stress exponent values: lower external stress leads to lower ability of dislocation movement, higher sensitivity and higher stress exponent values. Furthermore, the stress exponent values' increase with increasing Cr content, in contrast to the previous case, could possibly be attributed to the fact that the applied external stress may be sufficient to activate dislocation sliding phenomena, but not sufficient to activate the dislocation climbing mechanisms, something that is quite common in BCC structures due to its limited number of screw-type dislocations [12,18,22].

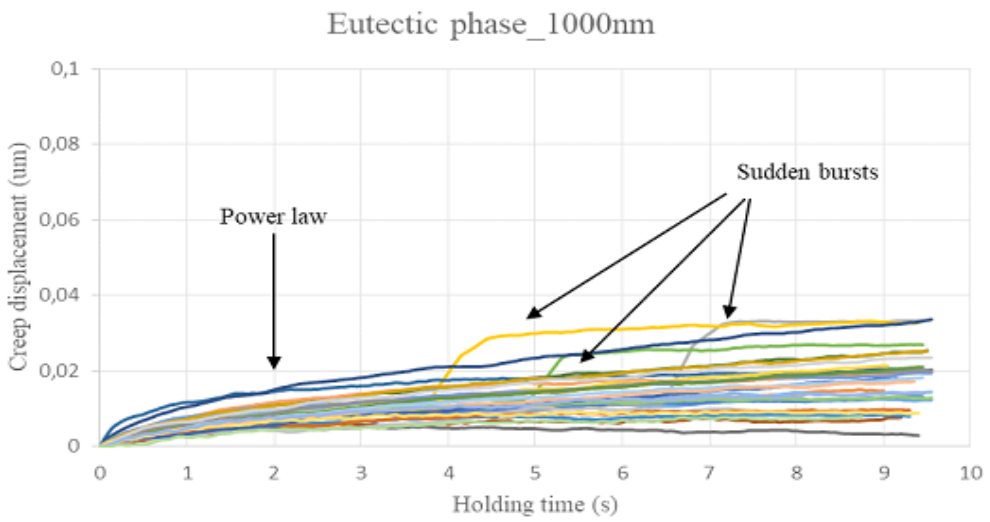


**Figure 15:** The indentation displacement as a function of time during the holding (creep) stage of the indentation tests for the eutectic phase at 1000 nm penetration depth

Table 5: Summarized values of creep displacement, lattice distortion and stress exponent for the eutectic and primary phases of all the examined alloys at 1000 nm penetration depth

| | | Creep displacement | Lattice distortion | Stress exponent |
|---|---|---|---|---|
| ***NiAl-25Cr*** | Eutectic | 18.53 ± 8 | - | 121.45 ± 3 |
| | Primary | 10.97 ± 2 | 6.70 | 102.79 ± 5 |
| ***NiAl-33Cr*** | Eutectic | 16.37 ± 6 | - | 105.07 ± 2 |
| | Primary | 17.07 ± 5 | 6.62 | 117.33 ± 5 |
| ***NiAl-40Cr*** | Eutectic | 17.61 ± 4 | - | 94.63 ± 2 |
| | Primary | - | - | - |
| ***NiAl-60Cr*** | Eutectic | - | - | - |
| | Primary | 15.16 ± 5 | 6.35 | 148.60 ± 7 |

As in the case of the eutectic phase at 500 nm depth, not a single mechanism describing the stress exponent values of the eutectic micro-constituent at 1000 nm depth, can be suggested. However, even in this case, it seems that the effect of the externally applied load is confirmed: the lower the applied load, the higher the stress exponent.

## Conclusion

The indentation modulus ($E_{IT}$), in the case of the alloys' primary constituent, shows a slight decrease in the NiAl-25Cr and NiAl-33Cr alloys, where the primary constituent consists of a NiAl-rich B2 phase. On the contrary, in the case of alloy NiAl-60Cr, the $E_{IT}$ value increases due to the presence of the intrinsically hard Cr-rich A2 primary phase. This trend governs both penetration depths (500 nm and 1000 nm) with the observation that in all systems the $E_{IT}$ decreases at 1000 nm depth.

In the case of the eutectic micro-constituent, the general trend for lower $E_{IT}$ values at higher penetration depths, is verified with the exception of the NiAl-33Cr alloy. The significant difference compared to the case of the primary components is the fact that the eutectic micro-constituent consists of nano-crystalline components and not a signle crystal.

Regarding the indentation micro-hardness of the primary phases, it seems that there are no major differences between the corresponding values of the NiAl-25Cr and the NiAl-33Cr alloys, while an although expected slight increase in micro-hardness in the case of alloy NiAl-60Cr is observed. As in the case of the indentation modulus, the values of micro-hardness decrease with increasing penetration depth, as well.

When the eutectic micro-constituent is concerned, observations similar to those of indentation modulus are made. In particular, the penetration depth seems to have a similar effect, however, the NiAl-33Cr system has the same behaviour as before, i.e. lower values and a reverse behaviour between the penetration depths.

In the case of the $n_{IT}$ ratio for the primary phase examination, it seems that all systems follow the trend that characterizes

both the indentation modulus and hardness: The higher the indentation modulus and hardness, the lower the energy due to elastic deformation. Another interesting point is the decrease of the ratio with the penetration depth, a fact that is completely expected, since with increasing the penetration depth, the area of plastic zone increases and so as the ratio. In the case of the eutectic micro-constituent, though, no specific tendency appears, which is probably attributed to the nano-structured morphology it displays.

The loading curves at 500 nm depth for both the primary and the eutectic phases, show a smooth evolution without localized gradations or small plateaus, which indicates that no creep occurs during the initial loading stage. Interestingly, the desired penetration depth (500 nm) in the case of the eutectic micro-constituent is achieved for smaller loads than those required for the primary phase.

Regarding the loading curves at 1000 nm depth, no difference in their morphology and shape is observed, compared to the previous case of 500 nm. Consequently, it could be said that this case is also governed by similar phenomena and mechanisms. In contrast to the case of 500 nm depth, however, in this case, the eutectic micro-constituent does not exhibit the same ability in obtaining the desired depth.

The creep displacement-time curves for the primary constituent at 500 nm depth showed that the majority of the curves exhibit a typical power law creep morphology, while at the same time in some individual cases, a sharp increase in creep deformation is also observed, which is known as "sudden bursts". Concerning the corresponding results for the eutectic micro-constituent, it was found that all curves follow the typical power law creep behaviour.

The creep displacement-time curves for the primary constituent at 1000 nm depth showed that all of them are governed by the power law. The corresponding curves for the eutectic micro-constituent at 1000 nm depth, however, show that the majority of them follows the power law creep behaviour, while there are some cases where a sharp increase in creep deformation is also observed.

The creep displacement analysis showed that the specific parameter increases from the NiAl-25Cr to the NiAl-33Cr alloy. In both systems, the primary constituent belongs to a NiAl-rich B2 phase. Consequently, as the displacement becomes bigger, the obstacles to the dislocation movement, which could provide plastic deformation, are increased, as well. As for the primary constituent of the NiAl-60Cr alloy, it cannot be compared to the previous cases, as it consists of a different Cr-rich A2 phase. As for the eutectic micro-constituent, the creep displacement values do not show significant differences.

The stress exponent values of the primary phase at 500 nm depth, shows a gradual decrease with increasing Cr content, while in the case of the eutectic micro-constituent the formulation of a mechanism explaining the changes in the stress exponent values is difficult to be conducted. The calculated values of the eutectic phase are generally lower than those of the primary phase, i.e. the creep deformation becomes easier. In the case of 1000 nm penetration depth the behaviour of the primary phase is reversed. More specifically, the increase of the Cr content leads to the increase of the stress exponent values, contrarily to the corresponding values at the penetration depth of 500 nm.

## Funding

This research is co-financed by Greece and the European Union (European Social Fund- ESF) through the Operational Programme « Human Resources Development, Education and Lifelong Learning » in the context of the project "Strengthening Human Resources Research Potential via Doctorate Research" (MIS-5000432), implemented by the State Scholarships Foundation (IKY). The raw/ processed data required to reproduce these findings cannot be shared at this time as the data also forms part of an ongoing study.

## References

1. Noebe RD, Bowman RR, Nathal MV. Physical and mechanical metallurgy of NiAl. 1994.
2. Tang, Cogswell, Xu S, Milenkovic, Cui Y. The formation mechanism of eutectic microstructures in NiAl–Cr composites. Phys Chem Chem Phys. 2016;18:19773–19786.
3. Takeuchi. Classification of Bulk Metallic Glasses by Atomic Size Difference, Heat of Mixing and Period of Constituent Elements and Its Application to Characterization of the Main Alloying Element. Mater Trans. 2005;46:2817–2829.
4. Locci, Dickerson, Garg, Noebe, Whittenberger, Nathal, Darolia. Microstructure and phase stability of single crystal NiAl alloyed with Hf and Zr. J Mater Res. 1996;11:3024–3038.
5. Miracle. Multiphase intermetallics. Acta Metall Mater. 1993;41:649–684.
6. Barabash, Liu, Tischler, Bei, Budai. Phase-specific elastic/plastic interface interactions in layered NiAl–Cr (Mo) structures. Acta Mater. 2012;60:3279–3286.
7. Chen, Tang, Kuo, Chen, Tsau, Shun, Yeh. Age Heat Treatment of the CoCrFeNiTi0.3 High-Entropy Alloy. Mater Sci Eng A. 2010;527:5818–5825.
8. Hsu, Juan, Sheu, Chen, Yeh. Effect of Aluminum Content on Microstructure and Mechanical Properties of Al (x) CoCrFeMo0.5Ni High-Entropy Alloys. 2013;65:1840–1847.
9. Hsu, Sheu, Yeh, Chen. Effect of iron content on wear behavior of AlCoCrFexMo0.5 Ni high-entropy alloys. 2010;286(5-6):653–659.
10. Wu JM, Lin SJ, Yeh JW, Chen SK, Huang YS, Chen HC. Adhesive wear behavior of AlxCoCrCuFeNi high-entropy alloys as a function of aluminum content. Wear. 261 (2006) 513–519
11. Ming HC, Ming HT, Woei RW, Jien Lin, Wei Y. Microstructure and wear behavior of AlxCo1. 5CrFeNi1. 5Tiy high-entropy alloys. Acta Mater. 59 (2011) 6308–6317.
12. Li WB, Henshall JL., Hooper RM, Easterling KE. The mechanisms of indentation creep. Acta Metall. Mater. 1991;39: 3099–3110.
13. Zhang L, Yu P, Cheng H, Zhang H, Diao H, Shi Y, et al. Nanoindentation creep behavior of an Al0.3CoCrFeNi high-entropy alloy. Metall Mater

Trans A. 2016;47:5871–5875

14. Ding ZY, Song YX, Ma Y, Huang XW, Zhang TH. Nanoindentation Investigation on the Size-Dependent Creep Behavior in a Zr-Cu-Ag-Al Bulk Metallic Glass. Metals. 2019;9:613.
15. Lin, Chou, Huang, Chuang, Jang, Nieh. Elevated-temperature creep of high-entropy alloys via nanoindentation MRS Bull. 2019;44:860–866.
16. Choi, Yoo, Kim, Jang. Indentation creep revisited. Mater Res. 2012;27:3–11.
17. Ma, ZS, Long, SG, Zhou, YC Indentation scale dependence of tip-in creep behavior in Ni thin films. Scr Mater. 2008;59:195–198.
18. Ma, Feng, Debela, Peng, Zhang. Nanoindentation study on the creep characteristics of high-entropy alloy films: fcc versus bcc structures. Int J Refract Met Hard Mater. 2016;54:395–400.
19. Mathiou, Giorspyros, Georgatis, Karantzalis. Microstructural verification of the theoretically predicted morphologies of the NiAl–Cr pseudo-binary alloy systems and NiAl–Cr eutectic structure modification by Mo addition. SN Applied Sciences. 2019;1:1-10
20. Karantzalis, Sioulas, Poulia, Mathiou, Georgatis. A first approach on the assessment of the creep behavior of MoTaNbVxTi high entropy alloys by indentation testing. SN Applied Sciences. 2020;1-10.
21. Jiao, Chu, Yang, Wang, Qiao. Nanoindentation characterised plastic deformation of a Al 0.5 CoCrFeNi high entropy alloy, Mater Sci Technol. 2015;31:1244–1249. doi:10.1179/1743284715Y.0000000048.
22. Wang, Guo, Wang, Liu, Wang, Yang, Liu. Nanoindentation characterized initial creep behavior of a high-entropy-based alloy CoFeNi. Intermetallics. 2014;53:183–186.
23. Bahr, Kramer, Gerberich. Non-linear deformation mechanisms during nanoindentation. Acta Mater. 1998;46:3605–3617.
24. Feng, Ngan. Creep and strain burst in indium and aluminium during nanoindentation. Scr Mater. 2001;45:971–976.